

Two-Channel Demultiplexer Based on 1D Photonic Star Waveguides Using Defect Resonators Modes

Youssef Ben-Ali^{1, 3, *}, Ilyass El Kadmiri¹, Amina Ghadban², Kamal Ghoumid², Abdelfattah Mazari¹, and Driss Bria¹

Abstract—In this work, we give a theoretical demonstration of the possibility to realize a photonic demultiplexer. The demultiplexer consists of Y-shaped waveguides with one input line and two output lines. We consider a demultiplexer composed of a segment and two asymmetric resonators, grafted at the same position in each channel. This system creates the resonance modes that have a maximum transmission rate and low Q quality factors. To improve these results, we take each output line consisting of a periodicity of segments and grafted at its extremities by a single resonator. Such a system creates passbands separated by band gaps. On the other hand, the presence of a resonator defect in the middle of each output line allows us to create defect modes inside the gaps. The results show that our proposed demultiplexer system manages to separate two incoming mixed signals of frequencies $f_1 = 204.75$ MHz and $f_2 = 208.75$ MHz and guide each one of them into two different channels.

1. INTRODUCTION

In communication networks, electromagnetic waves perform the crucial task of transferring information on very large distances with excellent speed and high quality factor [1–3]. In these networks, the electromagnetic waves move inside the channels (transmission lines) [4–9]. If you assign a channel to each user in a city with millions of users, you need a huge number of channel cables to cover all the users, which would be very expensive. The best solution to this problem is to assign a single channel to multiple users. Due to frequency division multiplexing (FDM) and dense frequency division multiplexing (DFDM) techniques, it is possible to transfer several electromagnetic waves (signals) with different frequencies or wavelengths inside a single channel. After transferring multiple channels in a single transmission line, it is necessary to have a device to separate these channels from each other and transmit them to the corresponding users [10, 11].

The photonic demultiplexer is able to separate multiple transmission lines with different frequencies or wavelengths. To make ultra-compact devices, the structures are needed to control the propagation of signals inside very small spaces. Due to their photonic band gap (PBG), the waveguides structures have an excellent ability to confine and control electromagnetic waves over a very important frequencies range, and therefore, these waveguides are very promising structures for designing compact electromagnetic devices such as filters, decoders, gates, switches drop-channel, and demultiplexers [12–14]. The number of output transmission lines, transmission efficiency, quality factor, crosstalk, and channel spacing are the most crucial features of demultiplexers.

Furthermore, several types of photonic, plasmonic, and phononic demultiplexers have been proposed for integrated technology. Ghorbanpour and Makouei have proposed a 2-channels demultiplexer based

Received 12 June 2021, Accepted 13 August 2021, Scheduled 23 August 2021

* Corresponding author: Youssef Ben-Ali (youssef.benali@usmba.ac.ma).

¹ Laboratory of Materials, Waves, Energy and Environment, Team of Acoustics, Photonics and Materials, Faculty of Sciences, Mohamed First University, Oujda, Morocco. ² Equipe des Signaux, Systèmes et Traitement de l'Information, Ecole Nationale des Sciences Appliquées d'Oujda, Université Mohamed I, Oujda 60000, Morocco. ³ Engineering Sciences Laboratory (LSI), Multidisciplinary Faculty of Taza, Sidi Mohamed Ben Abdellah University, B.P. 1223, Taza Gare, Morocco.

on photonic crystal ring resonator (PCRR). For performing wavelength selection, they have used two ring resonators; two different wavelengths were obtained by using two resonant rings with different values for the radius of dielectric rods. Results suggest that 2-channels in the proposed structure are characterized by high transmission efficiency and low bandwidth, resulting in a very sharp output spectrum and high quality factor values [15]. Rostami et al. have investigated a small size 4-channels wavelength division demultiplexer based on a 2D photonic crystal modified Y branch. The output wavelengths of designed structure can be tuned for communication applications by choosing suitable defect parameters in the corner of each resonance cavity and output waveguides [16]. Alipour-Banaei et al. have proposed a novel structure for designing optical demultiplexer based on a photonic crystal ring resonator. For performing wavelength selection task, they have used four ring resonators. The resonance wavelength of the ring resonators depends on the dimensions of the ring core; therefore, they have chosen two different values for the lattice constant of the ring resonators core section [17]. Azzazi and Swillam have proposed a nanoscale plasmonic demultiplexer based on a plasmonic slot resonator. The device is optimized for high selectivity and minimum FWHM (Full width at half maximum). The device is capable to achieve a demultiplexing FWHM of 9.8 nm for each channel with a high output transmission [18]. Khani et al. have investigated a plasmonic demultiplexers using improved circular nanodisk resonators (CNRs), and metal-insulator-metal (MIM) waveguides have been designed. The proposed structures use air and silver as insulator and metal layers, respectively. It is shown that increasing the CNRs radii for the single-mode bandpass filter (BPF) increases the resonance wavelength, linearly [19]. Xie et al. proposed a novel plasmonic demultiplexer in metal-insulator-metal (MIM) waveguide crossing with multiple side-coupled hexagonal resonators. Simulation results reveal that the demultiplexed wavelength, transmission efficiency, and bandwidth of each channel can be manipulated by adjusting structural parameters of the demultiplexer [20]. Mouadili et al. have given an analytical demonstration of the possibility to realize a simple phononic demultiplexer. The demultiplexer consists of a Y-shaped waveguide with an input line and two channels. Each channel contains two stubs (resonators) grafted either at a given position or at two positions far from the input line [21].

The design of the device based on a one-dimensional photonic periodic system (such as star waveguides consisting on coaxial cables) is extremely interesting for designers of integrated circuits used in the telecommunication field (filters, couplers, switches, etc.) [22–24]. Recent works show a great tendency in these photonic star waveguides because of their outstanding electromagnetic properties. In particular, they offer efficient ways of controlling the flow of electromagnetic waves by acting as an electromagnetic filter or by exhibiting absolute photonic band gaps in which the propagation of electromagnetic waves is prohibited [25, 26]. By focusing on the photonic band gap of this perfect system, it is possible to confine the electromagnetic waves at given frequencies. However, these perfect periodic photonic structures do not have the ability to select frequencies in these gaps. In this context, the defects insertion in these periodic structures gives rise to localized states inside these prohibited regions which permit to select very specific frequencies [22–24]. The presence of defects improves the interaction of electromagnetic waves with constituents of the structure because of their ability to create authorized states (defect modes) in band gaps. It is useful to use these defects to design the guides or filters [27–29]. In our previous works, we have examined the defective star waveguides structure with one output channel, and the effect of the most critical parameters in output spectra was investigated [2, 22–25].

In this paper, we illustrate the possibility of designing a FDM based on defect modes that propagate inside the band gaps. The proposed wired Y-shaped (coaxial cables) photonic demultiplexer consists of one-dimensional waveguides with one input line and two transmission lines (channels or output lines). Firstly (Fig. 1(a)), we take a structure which contains an input line and two output lines. The first output line contains a segment of length d_1 and two asymmetric resonators of lengths d_2 and d_3 inserted on the same site 2, and the second output contains a segment of length d_4 different from d_1 and two asymmetric resonators of lengths d_5 and d_6 grafted on the same site 3. This system creates large resonance modes (low quality factors) that have maximum transmissions. Secondly, we take a photonic demultiplexer constituted by an input line and two output lines in which the numbers of sites in the first and second output lines are respectively N and N' (Fig. 1(b)). The first output line 1 is composed by the periodicity of the segment of length d_1 and grafted in each site by one resonator of length d_2 , and the second output line is composed by the periodicity of the segment of length d_3 and grafted in

each site by one resonator of length d_4 . This kind of demultiplexer, which is based on the periodicity of transmission lines, is original. It represents the added value of this work in scientific literature. Thirdly, we take the demultiplexer represented in Fig. 1(b) and introduce a resonator defect of length d_2 in the site J for the first output line, and another resonator defect of length d_{04} is in the site J' for the second output line 2 (Fig. 1(c)). The main objective of this work is to efficiently filter and separate two frequencies (two signals or information) on two output lines (in different paths) with very high transmission rates and high quality factors for application in a telecommunications device. In this paper, we use the numerical method for the proposed demultiplexer. We use the Green function method for calculating the transmission and reflection rates of the waveguides structure. In all our calculations, we assume that the cross-section of the segments is small compared to its linear dimension (length). This assumption allows us to consider our proposed structure composed of segments and resonators as a one-dimensional (1D) system.

This paper is organized as follows. In Section 2, we perform the analytical calculation of transmission and reflection rates using the interface response theory which is based on the Green's function method for a photonic demultiplexer. The first simple demultiplexer is constituted by only one segment and two asymmetric resonators in each channel, while for the second proposed demultiplexer, each outline channel is composed of cells periodicity, and each cell is constituted by a segment and grafted by one resonator. We insert in each branch of the proposed demultiplexer a defect resonator of physical properties different from those composed of the periodic line. Section 3 gives the numerical results to achieve a complete transmission in one channel by canceling the transmission in the second channel as well as the reflection in the input line. Some parameters of the proposed structure are determined in this section. In Section 4, we present the main results of this paper.

2. THEORETICAL FORMALISM: INTERFACE RESPONSE THEORY (GREEN FUNCTION)

Green Function (GF) is among the most used methods for the analysis of electromagnetic waveguides structure. This method permits to calculate the different properties of the propagation of electromagnetic waves such as the dispersion relation, transmission, reflection spectra, and other characteristics.

2.1. Transmission and Reflection Rates through a Demultiplexer Containing Two Asymmetric Resonators in Each Output Line

In this section, we consider the structure proposed in Fig. 1(a). This system consists of an input line and two output lines, all attached point at the same site 1. The first output line contains one segment of length d_1 and two asymmetric resonators (stubs) of lengths d_2 and d_3 grafted at the same position 2 at a distance d_1 from the input line. Similarly, the second output line contains one segment of length d_4 and two asymmetric resonators of lengths d_5 and d_6 inserted on the same site 3 at a distance d_4 from the input line. The segments and resonators are composed by the coaxial cables (wired system) which are constituted by the same dielectric material. The calculation of transmission and reflection rates are realized by using the Green's function method. In this theory, the inverse of the Green's function of the whole system in the interfaces space $M = \{1, 2, 3\}$ is obtained from a superposition of the elementary constituents of the system.

The inverse of Green function of the three semi-infinite guides constituting the input line and two output lines is given by:

$$g_s^{-1}(1, 1) = g_s^{-1}(2, 2) = g_s^{-1}(3, 3) = -F_s \quad (1)$$

The inverse of Green function of the dangling resonators grafted at the sites $\{2\}$ and $\{3\}$ using the boundary condition at the ends of the resonators $H = 0$ (magnetic field equals zero) is given by:

$$g_i^{-1}(2, 2) = -\frac{F_2 S_2}{C_2} - \frac{F_3 S_3}{C_3} \quad \text{and} \quad g_i^{-1}(3, 3) = -\frac{F_5 S_5}{C_5} - \frac{F_6 S_6}{C_6} \quad (2)$$

where $C_i = \cosh(\alpha_i d_i)$; $S_i = \sinh(\alpha_i d_i)$; $\alpha_i = j \frac{\omega}{c} \sqrt{\varepsilon_i \mu_i}$; $F_i = \frac{\alpha_i}{\mu_i}$ and $j = \sqrt{-1}$.

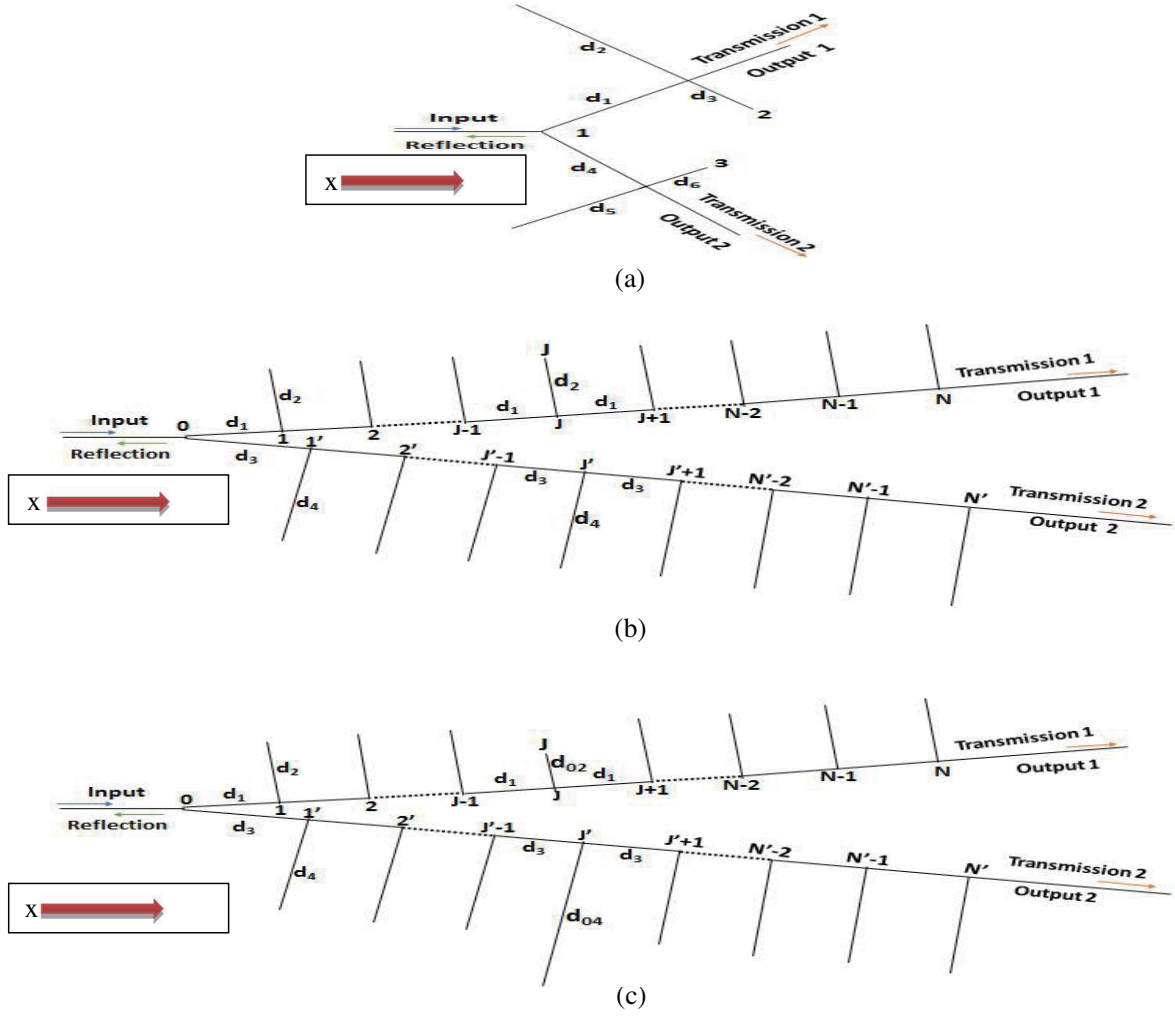


Figure 1. (a) Schematic representation of a Y-shaped demultiplexer with an input line and two output lines, all attached at the same point. Along the first output line, two resonators lengths d_2 and d_3 are inserted at a distance d_1 from the input line and along the second output line; two resonators of lengths d_5 and d_6 are inserted at a distance d_4 from the input line. (b) The first output line is composed of N periodic repetitions of cells built of the segment of length d_1 grafted in its extremity by a single resonator of length d_2 . The second output line 2 is composed of N' periodic repetitions of cells built of segments of length d_3 and grafted in its extremity by a single resonator of length d_4 . (c) is identical to the case shown in (b), except that the first output line contains a single resonator defect of length d_{02} located in the site J and the second output line contains a resonator defect of length d_{04} located in the site J' .

The inverse of Green function of segments of lengths d_1 and d_4 situated in the interfaces space $\{1, 2\}$ and $\{1, 3\}$ is given by following (2×2) matrix:

$$g_i^{-1}(1, 2) = g_i^{-1}(1, 3) = \begin{pmatrix} \frac{-F_i C_i}{S_i} & \frac{F_i}{S_i} \\ \frac{F_i}{S_i} & \frac{-F_i C_i}{S_i} \end{pmatrix} \quad \text{with } i = 1, 4 \quad (3)$$

We suppose that all the mediums (segments and resonators) have the same physical properties (i.e., $F_s = F_1 = F_2 = F_3 = F_4 = F_5 = F_6 = F$).

The inverse of the Green function of the composite structure in the interfaces space $M = \{1, 2, 3\}$

is given by the matrix (3×3):

$$g^{-1}(M, M) = -F \begin{pmatrix} 1 + \frac{C_1}{S_1} + \frac{C_4}{S_4} & -\frac{1}{S_1} & -\frac{1}{S_4} \\ -\frac{1}{S_1} & 1 + \frac{C_1}{S_1} + \frac{S_2}{C_2} + \frac{S_3}{C_3} & 0 \\ -\frac{1}{S_4} & 0 & 1 + \frac{C_4}{S_4} + \frac{S_5}{C_5} + \frac{S_6}{C_6} \end{pmatrix} \quad (4)$$

The reflection rate from the input line of the demultiplexer is:

$$R = |-1 - 2Fg(1, 1)|^2 = \left| -\frac{A + iB}{C + iD} \right|^2 \quad (5)$$

where:

$$A = C_2C_3C_5C_6(S_1S_4 - C_1C_4) + C_2C_3C_4S_1E + C_1C_5C_6S_4F + S_1S_4EF \quad (5a)$$

$$B = C_2C_3C_5C_6G + C_1C_2C_3C_4E + C_1C_4C_5C_6F - EFG \quad (5b)$$

$$C = 3C_2C_3C_5C_6(S_1S_4 - C_1C_4) + C_2C_3E(G + C_1S_4) + C_5C_6F(G + C_4S_1) - S_1S_4EF \quad (5c)$$

$$D = 3C_2C_3C_5C_6(C_4S_1 + C_1S_4) + (C_1C_4 - 2S_1S_4)(C_2C_3E + C_5C_6F) - EFG \quad (5d)$$

$$E = \sin(k(d_5 + d_6)); F = \sin(k(d_2 + d_3)); G = \sin(k(d_1 + d_4)) \quad (5e)$$

$k = \omega\sqrt{\varepsilon_1}/c$, where ω is the pulsation; ε_1 is the relative permittivity of the segment of length d_1 ; and c is the velocity of the electromagnetic waves in vacuum.

The transmission rates are given by:

$$T_1 = |-2Fg(1, 2)|^2 = \left| \frac{2C_2C_3(S_4E - C_4C_5C_6 + iC_5C_6S_4)}{C + iD} \right|^2 \quad (6)$$

$$T_2 = |-2Fg(1, 3)|^2 = \left| \frac{2C_5C_6(S_1F - C_1C_2C_3 + iC_2C_3S_1)}{C + iD} \right|^2 \quad (7)$$

2.2. Transmission and Reflection Rates through a Demultiplexer Made of Perfect Periodic Structures

In this part, let us consider the structure proposed in Fig. 1(b) by choosing $N = N' = 7$ (seven cells in each channel). These values of N and N' are largely sufficient for the two periodic systems (channels) to show stable band gaps in which the defect modes will appear. However, if we take values of N and N' greater than 7, the theoretical calculation becomes heavier and more complicated without having more important effect about the width of the band gaps. The first output line is formed by a periodicity of the segment of length d_1 along which a resonator of length d_2 is grafted in each site in the x direction. The position x in a cell between sites n and $n + 1$ is represented by the pair (n, x) , where x is a local coordinate $0 \leq x \leq d_1$, and d_1 represents in this case the period of the first output line. Similarly, the second output line contains a periodicity of segment of length d_3 along which a single resonator of length d_4 is branched in each site. For the sake of simplicity, the semi-infinite guides and all the guides and resonators are assumed to be constituted of the same material. To realize this finite system (Fig. 1(b)), we take an infinite system and do the following operations; one suppresses the segment linking the sites $n = -1$ and $n = 0$, and the sites $n = N$ and $n = N + 1$ in the first output line, and the segment located between the sites $n = -1$ and $n = 0$ and the sites $n = N'$ and $n = N' + 1$ in the second output line. However, to calculate the transmission and reflection rates, we need to know the inverse of the Green function of the whole system in the interfaces space $M = \{0, 1, 2, 3, 4, 5, 6, 7, 8, 9, 10, 11, 12, 13, 14\}$.

The inverse of the Green function of a semi-infinite waveguide constituting the input and the two output lines:

$$g_s^{-1}(0, 0) = g_s^{-1}(7, 7) = g_s^{-1}(7', 7') = -F_s \quad (8)$$

The inverse of the Green function of the dangling resonators (resonator of length d_2) grafted vertically at a given site $\{i = 1, 2, 3, 4, 5, 6, 7\}$ has the following expression:

$$g^{-1}(i, i) = -\frac{F_2 S_2}{C_2} \quad (9)$$

The inverse of the Green function of the dangling resonators (stubs of the length d_4) grafted vertically at a given site $\{i' = 1', 2', 3', 4', 5', 6', 7'\}$ is:

$$g^{-1}(i', i') = -\frac{F_4 S_4}{C_4} \quad (10)$$

The inverse of the Green function of the segments of length d_1 , bounded by two interfaces located between the sites $M' = \{0, 1\}; \{1, 2\}; \{2, 3\}; \{3, 4\}; \{4, 5\}; \{5, 6\}; \{6, 7\}$:

$$g^{-1}(M', M') = \begin{pmatrix} \frac{-F_1 C_1}{S_1} & \frac{F_1}{S_1} \\ \frac{F_1}{S_1} & \frac{-F_1 C_1}{S_1} \end{pmatrix} \quad (11)$$

and the inverse of the Green function of the guide of length d_3 in the interfaces space $M'' = \{0, 1'\}; \{1', 2'\}; \{2', 3'\}; \{3', 4'\}; \{4', 5'\}; \{5', 6'\}; \{6', 7'\}$ is given by:

$$g^{-1}(M'', M'') = \begin{pmatrix} \frac{-F_3 C_3}{S_3} & \frac{F_3}{S_3} \\ \frac{F_3}{S_3} & \frac{-F_3 C_3}{S_3} \end{pmatrix} \quad (12)$$

In the following, we assume that all mediums have the same physical characteristics (i.e., $F_1 = F_2 = F_3 = F_4 = F_5 = F$).

The expression of $g^{-1}(M, M)$ can be obtained from a linear superposition of the inverse Green function of the elementary constituents in the interfaces space $M = \{0, 1, 2, 3, 4, 5, 6, 7, 1', 2', 3', 4', 5', 6', 7'\}$ namely:

$$g^{-1}(M, M) = -F \begin{pmatrix} u & v & 0 & 0 & 0 & 0 & 0 & 0 & 0 & w & 0 & 0 & 0 & 0 & 0 & 0 \\ v & x & v & 0 & 0 & 0 & 0 & 0 & 0 & 0 & 0 & 0 & 0 & 0 & 0 & 0 \\ 0 & v & x & v & 0 & 0 & 0 & 0 & 0 & 0 & 0 & 0 & 0 & 0 & 0 & 0 \\ 0 & 0 & v & x & v & 0 & 0 & 0 & 0 & 0 & 0 & 0 & 0 & 0 & 0 & 0 \\ 0 & 0 & 0 & v & x & v & 0 & 0 & 0 & 0 & 0 & 0 & 0 & 0 & 0 & 0 \\ 0 & 0 & 0 & 0 & v & x & v & 0 & 0 & 0 & 0 & 0 & 0 & 0 & 0 & 0 \\ 0 & 0 & 0 & 0 & 0 & v & x & v & 0 & 0 & 0 & 0 & 0 & 0 & 0 & 0 \\ 0 & 0 & 0 & 0 & 0 & 0 & v & y & 0 & 0 & 0 & 0 & 0 & 0 & 0 & 0 \\ 0 & 0 & 0 & 0 & 0 & 0 & 0 & 0 & z & w & 0 & 0 & 0 & 0 & 0 & 0 \\ 0 & 0 & 0 & 0 & 0 & 0 & 0 & 0 & 0 & w & z & w & 0 & 0 & 0 & 0 \\ 0 & 0 & 0 & 0 & 0 & 0 & 0 & 0 & 0 & 0 & w & z & w & 0 & 0 & 0 \\ 0 & 0 & 0 & 0 & 0 & 0 & 0 & 0 & 0 & 0 & 0 & w & z & w & 0 & 0 \\ 0 & 0 & 0 & 0 & 0 & 0 & 0 & 0 & 0 & 0 & 0 & 0 & w & z & w & 0 \\ 0 & 0 & 0 & 0 & 0 & 0 & 0 & 0 & 0 & 0 & 0 & 0 & 0 & w & z & w \\ 0 & 0 & 0 & 0 & 0 & 0 & 0 & 0 & 0 & 0 & 0 & 0 & 0 & 0 & w & \beta \end{pmatrix} \quad (13)$$

where:

$$\left. \begin{aligned} u &= 1 + \frac{C_1}{S_1} + \frac{C_3}{S_3}; & v &= \frac{-1}{S_1} \\ w &= \frac{-1}{S_3}; & x &= \frac{S_2}{C_2} + \frac{2C_1}{S_1} \\ z &= \frac{S_4}{C_4} + \frac{2C_3}{S_3}; & y &= 1 + \frac{C_1}{S_1} + \frac{S_2}{C_2} \\ \beta &= 1 + \frac{C_3}{S_3} + \frac{S_4}{C_4} \end{aligned} \right\} \quad (14)$$

The dispersion relation is determined from the following equation:

$$\det[g^{-1}(K; M, M)] = 0 \quad (15)$$

The reflection rate in the input line of the photonic demultiplexer is given by:

$$R = |-1 - 2Fg(0, 0)|^2 \quad (16)$$

The transmission rates in the output lines are given by:

$$T_1 = |-2Fg(0, 7)|^2 \quad (17)$$

$$T_2 = |-2Fg(0, 7')|^2 \quad (18)$$

The reflection and transmission rates satisfy the energy conservation:

$$R + T_1 + T_2 = 1 \quad (19)$$

2.3. Transmission and Reflection Rates through a Photonic Demultiplexer Containing Two Defects at the Resonators Levels

In this section, we take seven cells in each channel ($N = N' = 7$), and we study the effect of the insertion of geometrical defects in the photonic demultiplexer system. For it, we analytically calculate the transmission and reflection rates through the structure proposed in Fig. 1(c). This structure contains an input line and two output lines, all connected at its extremities by three semi-infinite waveguides, each output line constituted by a periodicity of finite segment and one lateral branch (resonator) grafted in each site. The demultiplexer is composed of resonators (medium 2) of length d_2 grafted periodically with a spacing period d_1 on the first finite output line with the number of cells $N = 7$. Similarly, the second output line is composed by the resonator of length d_4 branched periodically with a spacing period d_3 with the number of cells $N' = 7$. For more simplification, the semi-infinite guides and the mediums of the demultiplexer are assumed to be constituted of the same material. In the first step, one suppresses the segment linking the sites $n = -1$ and $n = 0$, and the sites $n = N$ and $n = N + 1$ in the first output line and the segment located between the sites $n = -1$ and $n = 0$, $n = N'$ and $n = N' + 1$ in the second output line (Fig. 1(b)). In the second step, two geometrical resonators defects are created inside the structure by changing two resonators of lengths d_2 and d_4 situated at the sites $J = 4$ (associate with a resonator defect located in the first output line) and $J' = 4'$ (correspond to a resonator defect located in the second output line) respectively by another resonator of lengths d_{02} and d_{04} (Fig. 1(c)). Therefore, the disturbed states are $M_s = \{-1, 0, J, N, N + 1, J', N', N' + 1\}$.

The cleavage operator in the interfaces space M_s : $\vec{V}(M_s, M_s) = \overset{\leftrightarrow}{g}_d^{-1}(M_m, M_m) - \overset{\leftrightarrow}{g}^{-1}(M_m, M_m)$ is the following (8×8) square matrix defined in the interfaces domain constituted of sites $n = -1, 0, J, N, N + 1, J', N', N' + 1$, where $\overset{\leftrightarrow}{g}_d^{-1}(M_m, M_m)$ is the inverse of the Green function of the system containing defects, and $\overset{\leftrightarrow}{g}^{-1}(M_m, M_m)$ is the inverse Green function of the infinite perfect periodic structure in the interfaces space M_m . This matrix is formed by the superposition of the elements $g^{-1}(M_i, M_i)$ ($i = 1, 2, 3, 4$) which are in Equations (9), (10), (11), and (12).

The interfaces response operator $\vec{A}(M_s, M_s)$ is written as follows:

$$\vec{A}(M_s, M_s) = \sum_{M_s} \vec{V}(M_s, M_s) \vec{g}(M_s, M_s) \quad (20)$$

where $\vec{g}(M_s, M_s)$ is calculated using the Equation 7(a) in Ref. [24].

The operator $\vec{\Delta}(M_s, M_s)$ is given by:

$$\vec{\Delta}(M_s, M_s) = I(M_s, M_s) + \vec{A}(M_s, M_s) \quad (21)$$

with $I(M_s, M_s)$ being the identity matrix in the interfaces space M_s

After calculating the operator $\vec{\Delta}(M_s, M_s)$, let us write this operator in interfaces space $M_0 = \{0, J, N, J', N'\}$.

We calculate $\overset{\leftrightarrow}{d}(M_0M_0) = \overset{\leftrightarrow}{g}(M_0M_0)\overset{\leftrightarrow}{\Delta}^{-1}(M_0M_0)$ in the interfaces space M_0 , with $\overset{\leftrightarrow}{\Delta}^{-1}(M_0, M_0)$ being the inverse of the operator $\overset{\leftrightarrow}{\Delta}(M_0, M_0)$ and $\overset{\leftrightarrow}{g}(M_0M_0)$ calculated using Equation (7a) in [24].

The interfaces Green function $\overset{\leftrightarrow}{d}(M_0, M_0)$ for the photonic demultiplexer is defined in the interfaces space $M_0 = \{0, J, N, J', N'\}$ by the following matrix:

$$\overset{\leftrightarrow}{d}(M_0, M_0) = \begin{pmatrix} d_{11} & d_{12} & d_{13} & d_{14} & d_{15} \\ d_{21} & d_{22} & d_{23} & d_{24} & d_{25} \\ d_{31} & d_{32} & d_{33} & d_{34} & d_{35} \\ d_{41} & d_{42} & d_{43} & d_{44} & d_{45} \\ d_{51} & d_{52} & d_{53} & d_{54} & d_{55} \end{pmatrix} \quad (22)$$

We deduce the truncated matrix $\overset{\leftrightarrow}{d}_{tr}(M'_0, M'_0)$ in the interfaces space $M'_0 = \{0, N, N'\}$ which is written as follows:

$$\overset{\leftrightarrow}{d}_{tr}(M'_0, M'_0) = \begin{bmatrix} d_{11} & d_{13} & d_{15} \\ d_{31} & d_{33} & d_{35} \\ d_{51} & d_{53} & d_{55} \end{bmatrix} \quad (23)$$

The inverse of this matrix $\overset{\leftrightarrow}{d}_{tr}(M'_0, M'_0)$ is written as follows:

$$\overset{\leftrightarrow}{d}_{tr}^{-1}(M'_0, M'_0) = \begin{bmatrix} A_{11} & A_{12} & A_{13} \\ A_{21} & A_{22} & A_{23} \\ A_{31} & A_{32} & A_{33} \end{bmatrix} \quad (24)$$

Finally, the Green function of a finite photonic demultiplexer $\overset{\leftrightarrow}{d}_h(M'_0, M'_0)$ located between three semi-infinite waveguides:

$$\overset{\leftrightarrow}{d}_h(M'_0, M'_0) = \begin{bmatrix} A_{11}-F & A_{12} & A_{13} \\ A_{21} & A_{22}-F & A_{23} \\ A_{31} & A_{32} & A_{33}-F \end{bmatrix} \quad (25)$$

From where:

$$\overset{\leftrightarrow}{d}_h(M'_0, M'_0) = \frac{1}{\det[\overset{\leftrightarrow}{d}_h^{-1}(M'_0, M'_0)]} \begin{bmatrix} A & B & C \\ D & E & F \\ G & H & I \end{bmatrix} \quad (26)$$

with:

$$\left. \begin{aligned} \det \left[\overset{\leftrightarrow}{d}_h^{-1}(M'_0, M'_0) \right] &= - (A_{13})(A_{22}-F)(A_{31}) + (A_{12})(A_{23})(A_{31}) + (A_{13})(A_{21})(A_{32}) \\ &\quad - (A_{11}-F)(A_{23})(A_{32}) - (A_{12})(A_{21})(A_{33}-F) + (A_{11}-F)(A_{22}-F)(A_{33}-F) \\ A &= (A_{22}-F)(A_{33}-F) - (A_{23})(A_{32}) \\ B &= (A_{13})(A_{32}) - (A_{12})(A_{33}-F) \\ C &= (A_{12})(A_{23}) - (A_{13})(A_{22}-F) \\ D &= (A_{23})(A_{31}) - (A_{21})(A_{33}-F) \\ E &= (A_{11}-F)(A_{33}-F) - (A_{13})(A_{31}) \\ F &= (A_{13})(A_{21}) - (A_{11}-F)(A_{23}) \\ G &= (A_{21})(A_{32}) - (A_{22}-F)(A_{31}) \\ H &= (A_{12})(A_{31}) - (A_{11}-F)(A_{32}) \\ I &= (A_{11}-F)(A_{22}-F) - (A_{12})(A_{21}) \end{aligned} \right\} \quad (27)$$

The reflection rate in the input line through the structure is given by the following relation:

$$R = \left| -1 - 2F \overset{\leftrightarrow}{d}_h(0, 0) \right|^2 = \left| -1 - 2F \frac{A}{\det \left[\overset{\leftrightarrow}{d}_h^{-1}(M'_0, M'_0) \right]} \right|^2 \quad (28)$$

The two transmission rates in the output lines of the photonic demultiplexer are given by the following expressions:

$$T_1 = \left| -2F \overset{\leftrightarrow}{d}_h(0, N) \right|^2 = \left| -2F \frac{B}{\det \left[\overset{\leftrightarrow}{d}_h^{-1}(M'_0, M'_0) \right]} \right|^2 \quad (29)$$

$$T_2 = \left| -2F \overset{\leftrightarrow}{d}_h(0, N') \right|^2 = \left| -2F \frac{C}{\det \left[\overset{\leftrightarrow}{d}_h^{-1}(M'_0, M'_0) \right]} \right|^2 \quad (30)$$

The reflection and transmission rates satisfy the energy conservation:

$$R + T_1 + T_2 = 1 \quad (31)$$

3. RESULTS AND DISCUSSIONS

3.1. Demultiplexer Based on Large Resonance Modes

Firstly, we consider the system presented in Fig. 1(a), and we show, in Figs. 2(a)–(d), the transmission rates spectra T_1 through the first output line (red color), T_2 through the second output line (blue color), and the reflection rate R in the input line (green color) as a function of the reduced frequency Ω/π for different values of the parameters $\delta = d_3 - d_2 = \alpha D$ ($D = d_2 + d_3$). The boundary condition on the free surface of the resonators is $H = 0$, and the reduced frequency $\Omega = \frac{\omega d_1}{c} \sqrt{\varepsilon_1}$ is a dimensionless quantity with c being the speed of electromagnetic waves in a vacuum and ω representing the angular pulsation (s^{-1}). According to Fig. 2, one notices that when the transmission rate T_1 in the first output line reaches unity ($T_1 = 1$), the transmission in the second output line T_2 and the reflection R in the input line vanish (i.e., $T_2 = R = 0$). Similarly, we find that when the transmission T_2 reaches unity ($T_2 = 1$), the transmission in the first output line and the reflection in the input line take minimum values (i.e., $T_1 = R = 0$). At the same time, it is noted that there are cases where the reflection rate through the input line takes a maximum value ($R = 1$) while the transmission rates in the two channels are canceled ($T_1 = T_2 = 0$), which makes it possible to consider that our system can be used as a total reflection filter. The choice of these values of the resonators lengths plays a very important role to find resonances modes with a very high transmission rate and very low reflection rate or vice versa (inverse), which allows us to consider that our demultiplexer proposed under these conditions can behave like a filter either by total reflection or total transmission. These results show that the resonance modes (peaks) of the structure in the first output line (red color) always falls at the same values of the reduced frequency $\Omega = \pi$ for all values of $\delta = d_3 - d_2$ while the resonance mode in the second output line (blue color) shifts to high frequencies. The frequency shift between these modes is very important, which permits to avoid noise problems. These resonance modes are due to the interaction between the propagating incoming signals in the system and the resonant modes of the two asymmetric resonators in each transmission line. These results show that the lengths of asymmetric resonators constituting the electromagnetic demultiplexer should be chosen appropriately in order to transfer a frequency in one transmission line by keeping the other transmission line unaffected. This type of resonance mode has already been found for a phononic and photonic demultiplexer with two channels, and each channel is composed of one segment and two asymmetric resonators [30–32]. These resonance modes are wide, i.e., low quality factor Q (calculated from $Q = \Omega/\Delta\Omega$ where Ω is the central frequency of the mode, and $\Delta\Omega$ is the width to half height of this mode) which can be considered poor in terms of signal guiding and filtering [24]. Hence, we deduce the importance of using the periodicity of each output line.

3.2. Perfect Photonic Demultiplexer System with $d_2 = 0.5d_1$, $d_3 = 0.5d_1$, and $d_4 = d_1$

In this paragraph, we examine in Fig. 3 the evolution of the transmission rates through the two output lines and the reflection rate in the input line as a function of the reduced frequency Ω . The red color

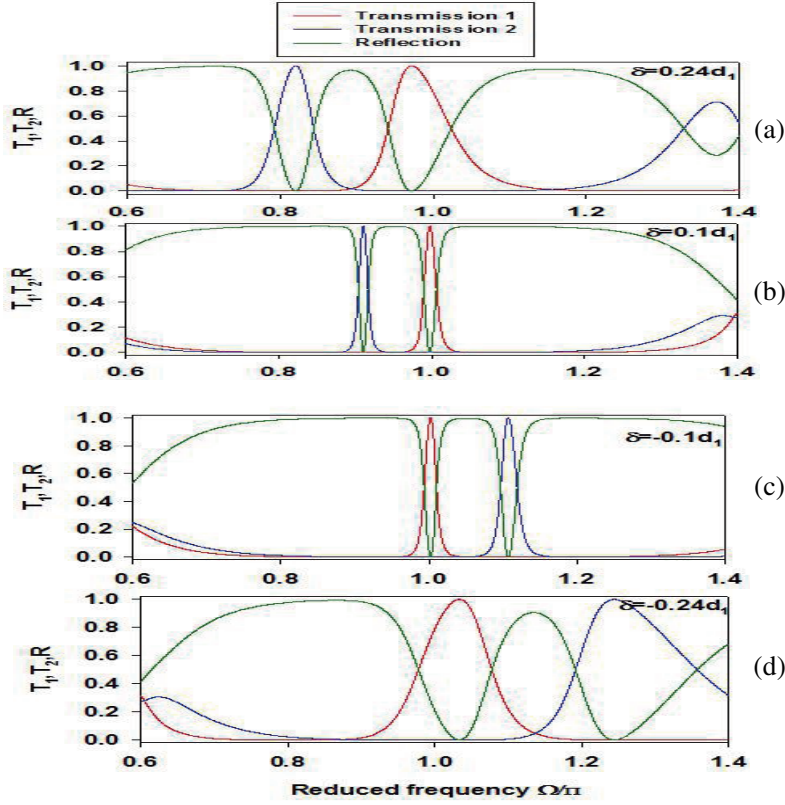


Figure 2. Variation of the signal transmitted in the first output channel (red color), in the second output channel (blue color) and the signal reflected in the input line of the demultiplexer (green color) as a function of the reduced frequency Ω/π for different values of δ , respectively (a) $\delta = d_3 - d_2 = 0.62D - 0.38D = 0.24D$, $d_1 = 0.62D$, $d_5 = d_4 = 0.5D$ and $d_6 = 0.74D$, (b) $\delta = 0.55D - 0.45D = 0.1D$, $d_1 = 0.55D$, $d_5 = d_4 = 0.5D$ and $d_6 = 0.6D$, (c) $\delta = 0.45D - 0.55D = -0.1D$, $d_1 = 0.45D$, $d_5 = d_4 = 0.5D$ and $d_6 = 0.4D$, (d) $\delta = 0.38D - 0.62D = -0.24D$, $d_1 = 0.38D$, $d_5 = d_4 = 0.5D$ and $d_6 = 0.26D$.

modes represent the variation of the transmission rate T_1 in the first output line (see Fig. 3(a)); the blue color modes show the transmission rate T_2 through the second output line (see Fig. 3(b)); and the green color modes represent the reflection through the input line. In Fig. 3(a), we observe that there are two wide complete band gaps (regions where the transmission rate equals zero) separated by three passbands. Fig. 3(b) shows that there are four complete band gaps separated by five passbands. Thus, we notice the existence of two passbands with $T_2 = 0$, and these pass bands are located around $\Omega = 4.7$ or $\Omega = 7.9$ when $T_2 = 0$. From Figs. 3(a)–3(b), it is evident that there are cases where the sum of the transmission rate in the pass bands equals 1, in which the incident signal coming from the input line is divided between the two output lines. The difference of gaps numbers in the two Figures is due to the ratio between the length of the resonator and the length of the segment in the first channel ($d_2/d_1 = 0.5$) and the same for the second channel ($d_4/d_3 = 2$). It is noticed from Fig. 3(c) that the reflection reaches unity ($R = 1$) when the transmission rates through the two output lines equal zero while $R = 0$ when the sum of the transmission rates through the two output lines reaches unity, or one of these two transmission rates equals 1. The appearance of these gaps is due to the periodicity of the system of each output line and the resonance states of the resonators. In the following, our objective is to create two very narrow defect modes inside these gaps in order to filter the localized modes of each defect resonator in the corresponding output line. The objective of choosing $N = 7$ and $N' = 7$ is due to the creation of large band gaps and to make it possible to control and manipulate the propagation of electromagnetic waves in a wide frequency range. Therefore, the defect modes are localized and confined inside these large forbidden bands with high performance.

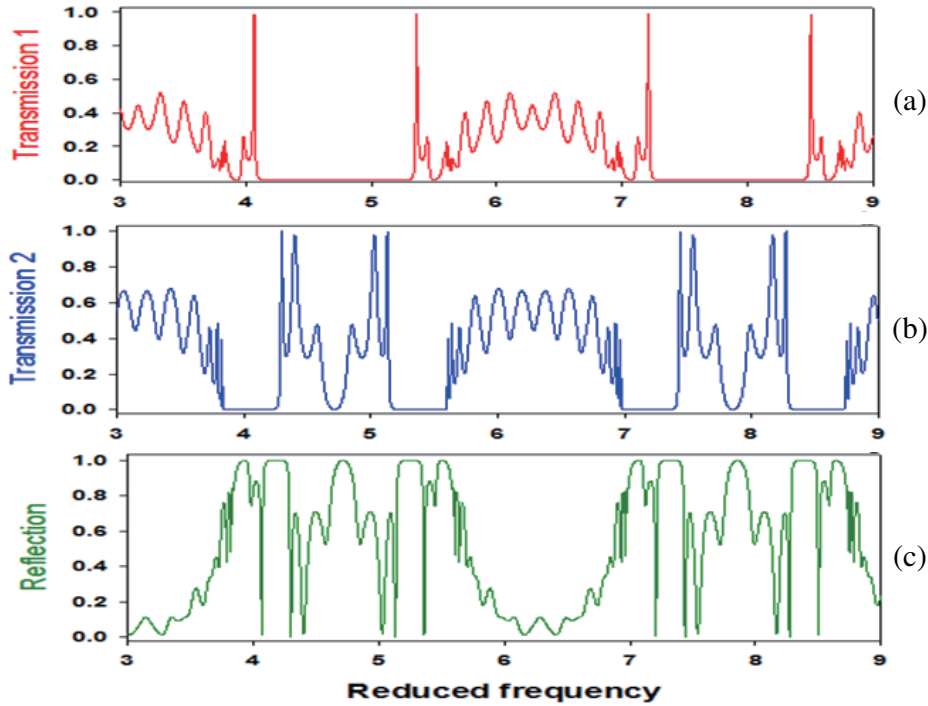


Figure 3. (a) Evolution of the transmission spectra in the output line of the perfect demultiplexer (red color) as a function of the reduced frequency Ω . (b) Transmission spectra in the second output line (blue color). (c) The reflection spectra through the input line (green color). We take $N = N' = 7$.

3.3. Photonic Demultiplexer Based on Defects Modes with $d_2 = 0.5d_1$, $d_3 = 0.5d_1$ and $d_4 = d_1$

3.3.1. Transmission Rates T_1 , T_2 and Reflection Rate R

In designing waveguides structure-based demultiplexers, the most crucial part is the frequency selection of the structure. In this structure, we use localized defect modes as the frequency selecting part of the demultiplexer. We consider a demultiplexer system consisting of an input line and two output lines which are studied in the previous paragraph (Section 3.2), and we create one defect resonator in each output channel, one defect resonator of length d_{02}/d_1 located in the middle of the first channel, and the second defect resonator of length d_{04}/d_1 located in the center of the second channel (See Fig. 1(c)). We then investigate, in Fig. 4, the variation of the transmission rate T_1 through the first output line, T_2 through the second output line and the reflection rate R through the input line as a function of the reduced frequency Ω for two values of d_{02}/d_1 and $d_{04} = 1.06d_1$. The choice of these values of the defect resonator lengths is very important for finding defect modes with a very high transmission rate and a very low reflection rate. Figs. 4(a)–4(b) show the variation of R (green color), T_1 (red color) and T_2 (blue color) as a function of the reduced frequency Ω corresponding to the interval of the large gap situated between $\Omega = 8$ and $\Omega = 8.8$. According to Figs. 4(a)–4(b), we observe the appearance of two peaks (modes), characterizing defects modes, which are situated in the middle of the photonic band gap; these two defects modes keep almost a very high value of transmission rate for the two values of d_{02}/d_1 . From Figs. 4(a)–4(b), it can be seen clearly that when the transmission rate in the first output line (Red color) reaches a very high value ($T_1 = 0.92$), the transmission rate in the second output line equals zero ($T_2 = 0$), and the reflection rate in the input line takes a very low value $R = 0.08$. Similarly, it is easy to see that when the transmission rate in the second output line reaches $T_2 = 0.95$ (Blue color), the transmission in the first output line equals zero ($T_1 = 0$, Red color), and the reflection rate takes a value of $R = 0.05$. The result also shows that the defect modes associated with the length d_{02}/d_1 move towards low frequencies when d_{02}/d_1 increases because these modes correspond to the

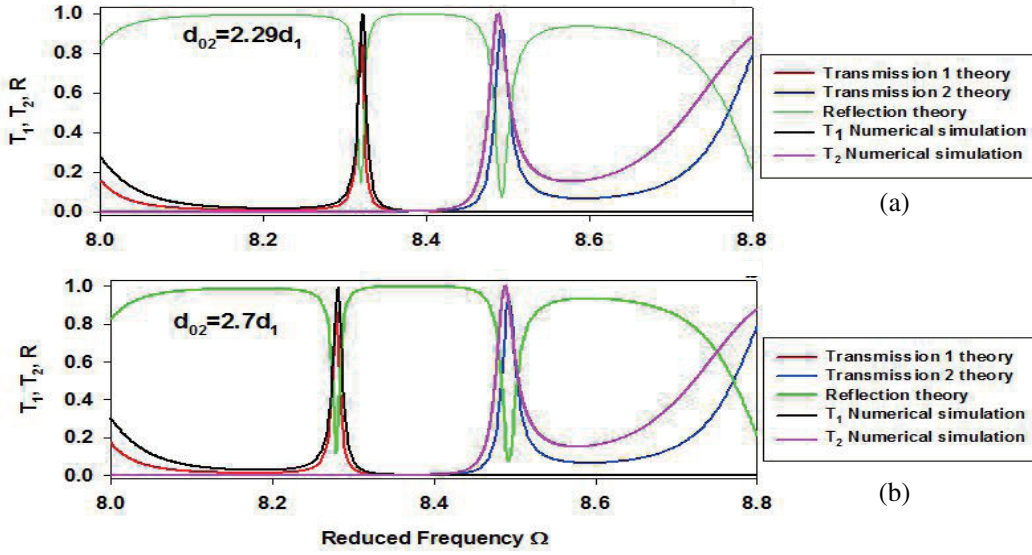


Figure 4. The transmittance spectra through the first output channel (red color), second output channel (blue color) and the reflection in the input line (green color) as a function of the reduced frequency Ω for two values of the defect length d_{02}/d_1 , respectively (a) $d_{02} = 2.29d_1$ and (b) $d_{02} = 2.7d_1$. The defect length associated to the channel 2 is $d_{04} = 1.06d_1$ and $N = N' = 7$.

defect of length d_{02}/d_1 unlike the other modes which are sensitive to the length d_{04}/d_1 . The black and pink modes are plotted numerically and correspond respectively to the two transmission rates T_1 and T_2 in each output line. These results show the compatibility between the analytical and numerical results. The presence of these defects modes in the gap is due to the interaction between the propagating signals in the system and the eigen modes of the defect resonator in each transmission line. The results of Figs. 4(a)–4(b) clearly show the possibility of filtering two frequencies in each output line. The interval between the filtered frequencies in each line depends on the difference between the lengths of two defect resonators. Hence, our proposed structure may be used as a double channels tunable FDM. Thus, we can extract any desired frequency by changing the defects resonators of lengths d_{04}/d_1 and d_{02}/d_1 . The results of these figures demonstrate that the defect resonator length in each channel should be chosen appropriately to transfer a frequency in one line by keeping the other line unaffected. So, two frequencies can be demultiplexed by using the structure shown in Fig. 1(c). Our objective is to propose an electromagnetic demultiplexer with a high transmission efficiency and high quality factor. The periodicity of the photonic structure and the insertion of a defect resonator in the middle of each output line more and more localize and confine the defect modes created in the band gaps of the photonic structure. To obtain well confined defect modes with a high quality factors Q , we need to broaden the band gaps of the periodic structure.

3.3.2. Color Map of Transmission Rates in Each Output Line

In the context of looking for regions where our demultiplexing system has a maximum transmission rate, we investigate in Figs. 5(a)–(b) a color map of the transmission rates in the two output lines as a function of both defect lengths d_{02}/d_1 and d_{04}/d_1 . The map is obtained by keeping, for every point of the plan (d_{02} and d_{04}), the maximum T_1 and T_2 of the transmission rates inside the gap. The red and purple colors indicate respectively high and low values of the transmission rates. By varying the resonators defects lengths at the same time, the transmitted power is changed. Note that the choice of the variation of these two defects lengths is made for the aim of finding regions where their transmission rates are very important. In regions where d_{02} varies between $2.1 \leq d_{02}/d_1 \leq 2.19$, or $2.38 \leq d_{02}/d_1 \leq 2.58$ or $2.77 \leq d_{02}/d_1 \leq 2.8$, we note that for some ranges of d_{04}/d_1 (red regions), the transmission rate in the first output channel is minimal, while it is maximum in the second output channel. Similarly, it seems that

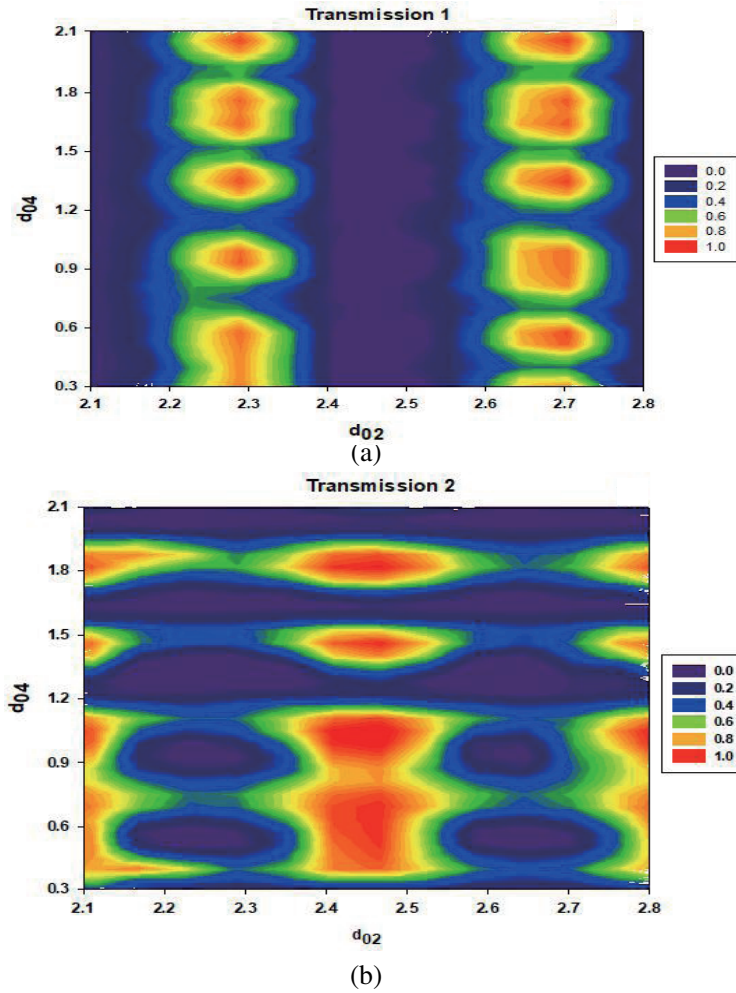


Figure 5. (a) and (b) represent the color maps of the transmission rates T_1 and T_2 as a function of the defect lengths d_{02}/d_1 and d_{04}/d_1 associated respectively to the first and second channels with $N = N' = 7$.

there are regions of d_{04} where the transmission in the two output channels is minimal (purple regions), which shows that there is a total reflection in the input line (for example when $2.38 \leq d_{02}/d_1 \leq 2.58$ and $1.6 \leq d_{04}/d_1 \leq 1.7$), and therefore we can use our demultiplexer in these regions as a total reflection filter [33–36]. In addition, we observe that the sum of the transmission rates is maximum ($T_1 = T_2 = 0.5$) for specific ranges of defective resonator lengths d_{02}/d_1 and d_{04}/d_1 ; this means that the energy of the electromagnetic waves is divided into two output channels with the same quantity (green regions). So, from Fig. 5, we conclude that the characteristics of the proposed demultiplexer in this paper meet the requirements of FDM applications [38, 39].

3.4. Demultiplexer Based on Defect Modes with $d_2 = 0.5d_1$, $d_3 = 1d_1$, and $d_4 = 0.5d_1$

3.4.1. Transmissions Spectrum T_1 , T_2 and Reflection Spectrums R

In this section, we illustrate the change of the defect lengths d_{02}/d_1 and d_{04}/d_1 on the defect modes behavior located in the gap. Figs. 6(a), 6(b), and 6(c) respectively represent the transmittance spectra through the transmission line 1 (red color), transmission line 2 (blue color), and the variation of the reflection rate (green color) for different values of d_{02}/d_1 by fixing the other defect length at $d_{04} = 0.7d_1$. According to the three figures, we indicate the appearance of two defect modes inside the band gap;

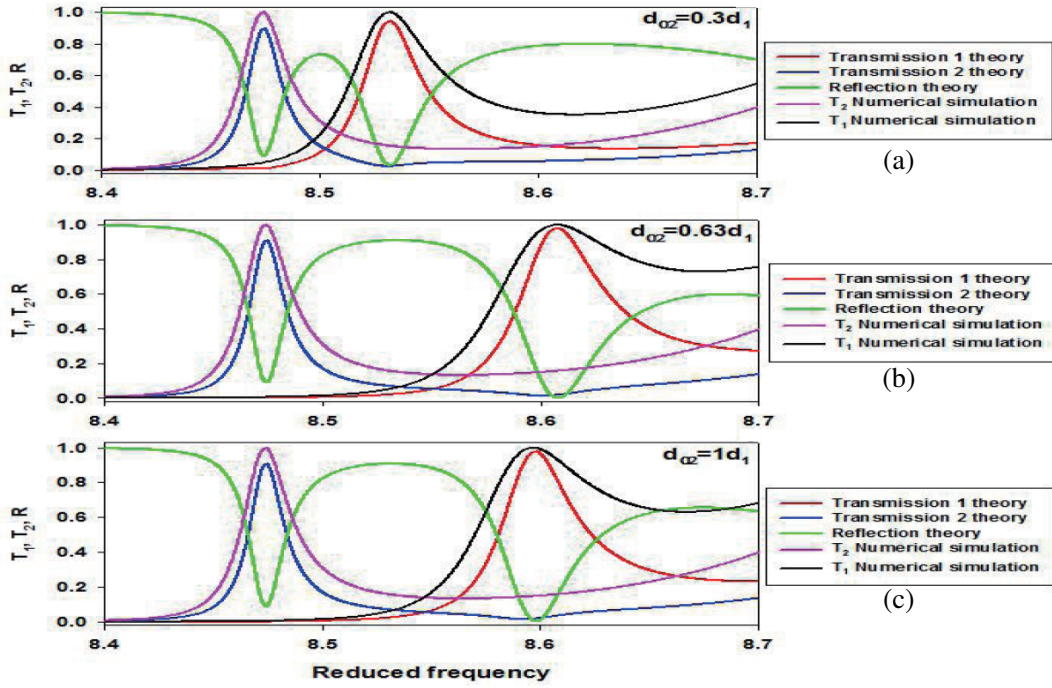


Figure 6. Transmission rates through the first output channel (red color), through the second output channel (blue color) and the variation of the reflection rate in the input line (green color) as a function of the reduced frequency Ω for three values of the defect length d_{02} , (a) $d_{02} = 0.3d_1$, (b) $d_{02} = 0.63d_1$ and (c) $d_{02} = 1d_1$. We fix the defect length $d_{04} = 0.7d_1$ and $N = N' = 7$.

these two modes have a very high transmission rate for the three values of d_{02}/d_1 . Fig. 6(a) clearly shows that when the transmission rate in the first output line is very important (i.e., $T_1 = 0.965$), the transmission rate in the second output line vanishes to $T_2 = 0$ while the reflection rate in the input line has a very low value (i.e., $R = 0.035$). On the other hand, when the transmission rate is $T_2 = 0.95$, the reflection $R = 0.05$ and transmission rate correspond to $T_1 = 0$. According to Fig. 6(b), we find that when the transmission rate in the first output line is very high (i.e., $T_1 = 0.99$), the transmission rate in the second output line takes a very low value $T_2 = 0.01$ while the reflection rate in the input line equals zero (i.e., $R = 0$). Similarly, we observe that when the transmission rate is $T_2 = 0.95$, the reflection $R = 0.05$ and transmission rate correspond to $T_1 = 0$. Also from Fig. 6(c), we note that when the transmission rate in the second output line reaches $T_2 = 0.945$, the transmission rate in the first line equals zero ($T_1 = 0$), and the reflection rate is characterized by a low value (i.e., $R = 0.055$). Also, we can see that when the transmission rate is $T_2 = 0.95$, the reflection $R = 0.05$ and transmission rate correspond to $T_1 = 0$. It should be noted that the frequency of the first defect mode (red color) increases progressively when the length d_{02}/d_1 is increased while the other defect mode (blue color) keeps the same value of the frequency. The features of the transmission of the very narrow defect modes found in these results present a solid foundation of a high performance demultiplexer. In order to compare our analytical results and numerical simulations, we find that the central frequencies of the defect modes are well verified and compatible between the numerical and analytical results. Comparing the results of Fig. 6 and Fig. 4, we conclude that the geometrical parameters (the lengths of the segments and the resonators in each channel) of the perfect demultiplexer change the frequencies of the defect modes within the band gaps.

Now, we display in Figs. 7(a)–7(c) the transmission rates T (Red color), T_2 (Blue color), and the reflection rate R (Green color) of the electromagnetic modes as a function of the reduced frequency for three values of d_{04}/d_1 . We observe the appearance of two defect modes inside the gap; these two modes keep very significant values of the transmission rate for three values of d_{04}/d_1 . Besides, we notice that when the transmission T_2 in the second output line reaches $T_2 = 0.99$, the reflection becomes zero

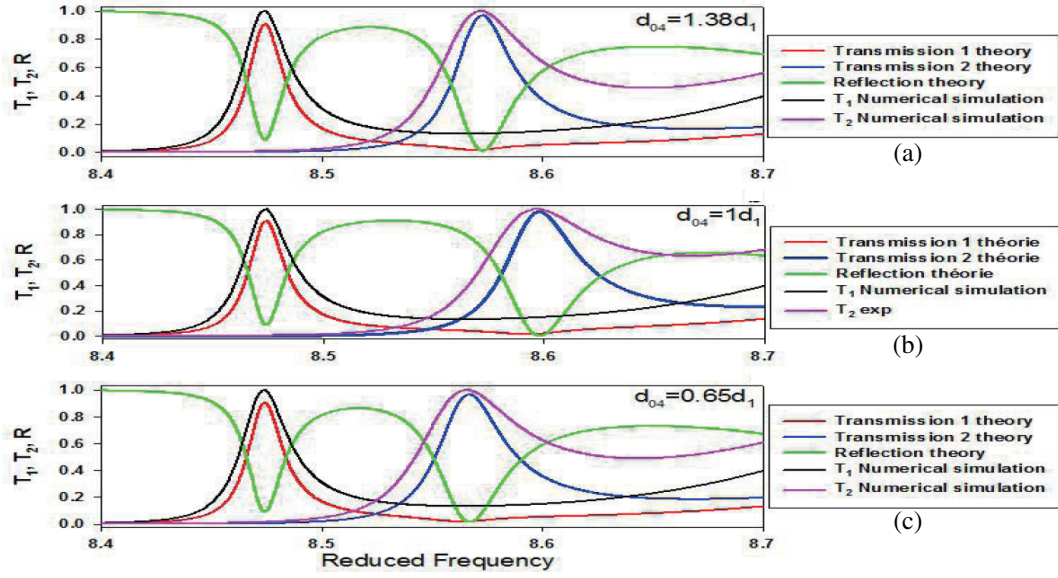


Figure 7. Transmission rates through the first output channel (red color), through the second output channel (blue color) and the variation of the reflection rate in the input line (green color) as a function of the reduced frequency Ω for three values of the defect length d_{04} , (a) $d_{04} = 1.38d_1$, (b) $d_{04} = 1d_1$, and (c) $d_{04} = 0.65d_1$. We fix the defect length $d_{02} = 0.698d_1$ and $N = N' = 7$.

$R = 0$, and the transmission in the first output line is $T_1 = 0.01$. In a similar way, we remark that when the transmission in the first output line reaches $T_1 = 0.965$, the transmission in the second line vanishes ($T_2 = 0$), and the reflection has a low value $R = 0.035$. We also validate our theoretical results with numerical simulation (black and pink color), and we find a good agreement. According to Figs. 4, 6, and 7 and in order to separate two channels with different frequencies, the resonators should have different lengths. Figs. 6 and 7 clearly show the strong effect of two defect lengths to realize a very high transmission rate. These two figures also show that the separation between the frequencies of the filter on each line depends on the difference between the lengths of the two defect resonators.

3.4.2. Color Map of Transmission Rates in Each Output Line

For a careful analysis of the transmission rates through the two channels, we present in Fig. 8 color maps of the transmission rates T_1 (Fig. 8(a)) and T_2 (Fig. 8(b)) as a function of both lengths of the two defects. The red and purple colors indicate, respectively, high and low values of the transmission rates. Figs. 8(a)–8(b) show that when d_2/d_1 varies between $0.6 \leq d_{02}/d_1 \leq 0.75$ and for all possible values of d_{04}/d_1 except d_{04}/d_1 varying between $0.66 \leq d_{04}/d_1 \leq 0.75$, the transmission rate of defect modes is maximal through the first output line (Transmission 1). We also note that when d_{04}/d_1 varies between $0.6 \leq d_{04}/d_1 \leq 0.75$ and for all possible values of d_{02}/d_1 except when d_{02}/d_1 varies between $0.68 \leq d_{02}/d_1 \leq 0.775$, the transmission rate of defect modes is maximal through the second output line (Transmission 2). To give a real illustration of our analytical and numerical results, and for the sake of comparison with previous experimental and theoretical works [30] concerning the electromagnetic demultiplexing process, we choose the following demultiplexer parameters: for Channel (1): $d_1 = 0.5$ m, $d_2 = 0.25$ m, $d_{02} = 0.315$ m and for Channel (2): $d_3 = 0.25$ m, $d_4 = 0.5$ m and $d_{04} = 0.33$ m. With this appropriate choice of the demultiplexer parameters, two mixed signals of frequency $f_1 = 204.75$ MHz and $f_2 = 208.75$ MHz, propagating through the input of our proposed photonic demultiplexer, will propagate separately in Channel (1) and Channel (2), respectively. The two demultiplexed signals are transmitted through the two output lines with 100% of transmission rate without any loss of information. Moreover, the band gaps shown by the two channels of the proposed structure impose more confinement on the transmitted signal by each channel. These two signals show a very small value of the half height which

leads to very important values of the quality factor.

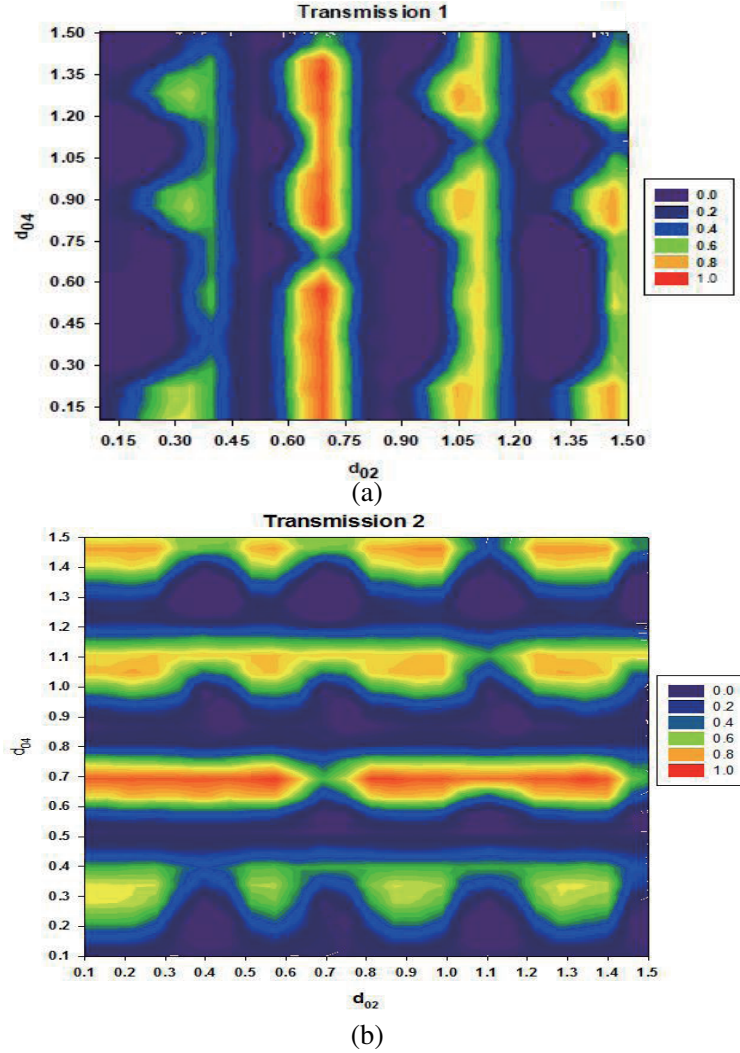


Figure 8. Color map of the transmitted rates T_1 (case a) and T_2 (case b) as functions of both the resonators defects length d_{02}/d_1 and d_{04}/d_1 associated respectively to the first and second output line. With $N = N' = 7$.

4. CONCLUSION

In this paper, we have studied a Y-shaped demultiplexer device consisting of an input line and two output lines (Transmission lines or Channels). For the sake of comparison, we have considered the case of demultiplexer with two different output channels, and each one of them is built by only one segment grafted in its extremity by two asymmetric resonators. The sizes of the components of the two simple channels are different. Such a system shows resonant modes (peaks) with very important transmission rates but with low quality factors. The choice of the lengths of the resonators and segments in this structure allows us to obtain given resonance frequency on one output line by keeping the other output line unaffected. To improve the quality factors of the two transmitted signals, we consider a Y-shaped demultiplexer in which each output line is composed by photonic star waveguides with resonator defect inserted in its middle. Due to the periodicity of the photonic channel which composed our demultiplexer, localized defect modes induced by the resonators defect appear in the large photonic band

gaps associated with each channel. This demultiplexer system with maximum transmission rates can be utilized for separating two incident mixed signals of frequencies $f_1 = 204.75$ MHz and $f_2 = 208.75$ MHz and guide each one of them into the first channel (1) and the second channel (2), respectively. The first channel is composed of periodic star waveguides containing $N = 7$ repetitions of segment of length $d_1 = 0.5$ m, grafted in each site by one resonator of length $d_2 = 0.25$ m, containing in its middle a resonator defect of length $d_{02} = 0.315$ m, while the second channel is constituted by periodic star waveguides containing $N' = 7$ repetitions of segment of length $d_3 = 0.25$ m grafted in its extremity by resonator of length $d_4 = 0.5$ m, and containing in its middle a defect resonator of length $d_{04} = 0.33$ m. Furthermore, our photonic demultiplexer, which is a system composed of two periodic output lines, is more efficient, in terms of sensitivity and transmission, than the simple demultiplexer system contained in each output line only by one segment and two asymmetric resonators (Section 3.1). The experimental results can be easily validated by simple experiments in the microwave frequency range [26].

ACKNOWLEDGMENT

We thank Mr. Youssef Farres (American Space Oujda, 60000, Morocco) for his valuable comments, notes and the critical reading and English language correction of our manuscript.

REFERENCES

1. Keshavarz, S., R. Keshavarz, and A. Abdipour, "Compact active duplexer based on CSRR and interdigital loaded microstrip coupled lines for LTE application," *Progress In Electromagnetics Research C*, Vol. 109, 27–37, 2012.
2. Ben-ali, Y., I. El Kadmiri, Z. Tahri, and D. Bria, "Defects modes in one-dimensional photonic filter star waveguide structure," *Materials Today: Proceeding*, Vol. 27, 3042–3050, 2020.
3. Keshavarz, S., A. Abdipour, A. Mohammadi, and R. Keshavarz, "Design and implementation of low loss and compact microstrip triplexer using CSRR loaded coupled lines," *AEU-International Journal of Electronics and Communications*, Vol. 111, 152913–152913, 2019.
4. Tan, W., Y. Sun, Z. G. Wang, and H. Chen, "Propagation of photons in metallic chain through side-branch resonators," *Journal of Physics D: Applied Physics*, Vol. 44, 335101–335106, 2011.
5. Tan, W., Z. G. Wang, and H. Chen, "Complete tuning of light through mu-negative media," *Progress In Electromagnetics Research M*, Vol. 8, 27–37, 2009.
6. Cocolozzi, G., H. L. Dobrzynski, B. Djafari-Rouhani, H. Al-Wahsh, and D. Bria, "Electromagnetic wave propagation in quasi-one-dimensional comb-like structures made up of dissipative negative-phase-velocity materials," *Journal of Physics: Condensed Matter, J. Phys, Condens. Matter*, Vol. 18, 3683–3690, 2006.
7. Yin, C. P. and H. Z. Wang, "Narrow transmission bands of quasi-1D comb-like photonic waveguides containing negative index materials," *Physics Letters. A*, Vol. 373, 1093–1096, 2009.
8. Weng, Y., Z. G. Wang, and H. Chen, "Band structure of comb-like photonic crystals containing metamaterial," *Optics communications*, Vol. 277, 80–83, 2007.
9. Zhang, L., Z. Wang, H. Chen, H. Li, and Y. Zhang, "Experimental study of quasi-one-dimensional comb-like photonic crystals containing left-handed material," *Optics communications*, Vol. 281, 3681–3685, 2008.
10. Keshavarz, S. and N. Nozhat, "Dual-band Wilkinson power divider based on composite right/left-handed transmission lines," *2016 13th International Conference on Electrical Engineering/Electronics, Computer, Telecommunications and Information Technology (ECTI-CON)*, 1–4, 2016.
11. Ghoumid, K., A. Ghadban, S. Boukricha, E. M. Arreyouchi, R. Yahiaoui, S. Mekaoui, and M. Raschetti, "Spectral coded phase bipolar OCDMA technological implementation thanks to low index modulation filters," *Telecommunication Systems*, Vol. 73, 433–441, 2020.
12. Studenkov, P. V., M. R. Gokhale, W. Lin, I. Glesk, P. R. Prucnal, and S. R. Forrest, "Monolithic

- integration of an all-optical Mach-Zehnderdemultiplexer using an asymmetric twin-waveguide structure,” *IEEE Photonics Technology Letters*, Vol. 13, 600–602, 2011.
13. Ghoumid, K., B. E. Benkelfat, R. Ferrière, and T. Gharbi, “Wavelength-selective Ti:LiNbO₃ multiple Y-branch coupler based on focused ion beam milled bragg reflectors,” *Journal of lightwave technology*, Vol. 29, 3536–3541, 2011.
 14. Fukazawa, T., F. Ohno, and T. Baba, “Very compact arrayed-waveguide-grating demultiplexer using Si photonic wire waveguides,” *Japanese Journal of Applied Physics*, Vol. 43, L673–L677, 2004.
 15. Ghorbanpour, H. and S. Makouei, “2-channel all optical demultiplexer based on photonic crystal ring resonator,” *Frontiers of Optoelectronics*, Vol. 6, 224–227, 2013.
 16. Rostami, A., H. Alipour Banaei, F. Nazari, and A. Bahrami, “An ultra compact photonic crystal wavelength division demultiplexer using resonance cavities in a modified Y-branch structure,” *Optik*, Vol. 122, 1481–1485, 2010.
 17. Alipour-Banaei, H., S. Serajmohammadi, and F. Mehdizadeh, “Optical wavelength demultiplexer based on photonic crystal ring resonators,” *Photonic Network Communications*, Vol. 29, 146–150, 2014.
 18. Azzazi, A. and M. A. Swillam, “Nanoscale highly selective plasmonic quad wavelength demultiplexer based on a metal–insulator–metal,” *Optics Communications*, Vol. 344, 106–112, 2015.
 19. Khani, S., M. Danaie, and P. Rezaei, “Double and triple-wavelength plasmonicdemultiplexers based on improved circular nanodisk resonators,” *Optical Engineering*, Vol. 57, 107102–107112, 2018
 20. Xie, Y. Y., C. He, J. C. Li, T. T. Song, Z. D. Zhang, and Q. R. Mao, “Theoretical investigation of a plasmonic demultiplexer in MIM waveguide crossing with multiple side-coupled hexagonal resonators,” *IEEE Photonics Journal*, Vol. 8, 84802512–84802520, 2016.
 21. Mouadili, A., E. H. El Boudouti, and B. Djafari-Rouhani, “Acoustic demultiplexer based on Fano and induced transparency resonances in slender tubes,” *European Physical Journal — Applied Physics*, Vol. 20, 1–8, 2020.
 22. Ben-ali, Y., Z. Tahri, F. Falyouni, and D. Bria, “Study about a filter using a resonator defect in a one- dimensional photonic comb containing a left-hand material,” *ICEERE*, Vol. 519, 146–156, 2018.
 23. Ben-ali, Y., Z. Tahri, A. Ouariach, and D. Bria, “Double frequency filtering by photonic comb-like,” *2018 International Symposium on Advanced Electrical and Communication Technologies (ISAECT)*, 2019.
 24. Ben-Ali, Y., Z. Tahri, and D. Bria, “Electromagnetic filters based on a single negative photonic comb-like structure,” *Progress In Electromagnetics Research*, Vol. 92, 41–56, 2019.
 25. Ben-ali, Y., A. Ghadban, Z. Tahri, K. Ghoumid, and D. Bria, “Accordable filters by defect modes in single and double negative star waveguides grafted dedicated to electromagnetic communications applications,” *Journal of electromagnetic waves and applications*, Vol. 34, 1–20, 2020.
 26. Dolorzynski, L., A. Akjouj, B. Djafari-Rouhani, J. O. Vasseur, and J. Zemmouri, “Giant gaps in photonic band structures,” *Phys. Rev. B*, Vol. 57, 9388–9391, 1998.
 27. Djafari Rouhani, B., J. O. Vasseur, A. Akjouj, L. Dobrzynski, M. S. Kushwaha, P. Deymier, and J. Zemmouri, “Giant stop bands and defect modes in one-dimensional waveguide with dangling side branches,” *Progress in Surface Science*, Vol. 59, 255–264, 1998.
 28. Djafari-Rouhani, B., E. H. El Boudouti, A. Akjouj, L. Dobrzynski, J. O. Vasseur, A. Mir, N. Fettouhi, and J. Zemmouri, “Surface states in one-dimensional photonic band gap structures,” *Vacuum*, Vol. 63, 177–183, 2001.
 29. Vasseur, J. O., P. A. Deymier, L. Dolorzynski, B. Djafari-Rouhani, and A. F. Akjouj, “Defect modes in one-dimensional comblike photonic waveguides,” *Phys. Rev. B*, Vol. 59, 13446–13452, 1999.
 30. Mouadili, A., E. H. El Boudouti, A. Soltani, A. Talbi, K. Haddadi, A. Akjouj, and B. Djafari-Rouhani, “Photonic demultiplexer based on electromagnetically induced transparency resonances,” *Journal of Physics D: Applied Physics*, Vol. 52, 075101–075125, 2018.

31. El Kadmiri, I., Y. Ben-Ali, A. Khaled, and D. Bria, “Y-shaped branch structure using asymmetric resonators for phononic demultiplexing,” *Materials Today: Proceedings*, Vol. 27, 3033–3041, 2020.
32. Mouadili, A., E. H. El Boudouti, and B. Djafari-Rouhani, “Acoustic demultiplexer based on Fano and induced transparency resonances in slender tube,” *European Physical Journal — Applied Physics*, Vol. 90, 1–8, 2020.
33. Borgese, L., M. Salmistraro, A. Gianoncelli, A. Zacco, R. Lucchini, N. Zimmerman, and E. Bontempi, “Airborne particulate matter (PM) filter analysis and modeling by total reflection X-ray fluorescence (TXRF) and X-ray standing wave (XSW),” *Talanta*, Vol. 27, R713–R715, 2011.
34. Soltani, A., T. Probst, S. F. Busch, M. Schwerdtfeger, E. Castro-Camus, and M. Koch, “Error from delay drift in terahertz attenuated total reflection spectroscopy,” *Journal of Infrared, Millimeter, and Terahertz Waves*, Vol. 35, 468–477, 2014.
35. Hands, J. R., K. M. Dorling, P. Abel, K. M. Ashton, A. Brodbelt, C. Davis, and M. J. Baker, “Attenuated total reflection Fourier transform infrared (ATR-FTIR) spectral discrimination of brain tumour severity from serum samples,” *Journal of biophotonics*, Vol. 7, 189–199, 2014.
36. Anderson, N. R. and R. E. Camley, “Attenuated total reflection study of bulk and surface polaritons in antiferromagnets and hexagonal ferrites: Propagation at arbitrary angles,” *J. Appl. Phys.*, Vol. 113, 013904–013917, 2013.
37. Ouchani, N., D. Bria, B. Djafari-Rouhani, and A. Nougouai, “Transverse-electric/transverse-magnetic polarization converter using 1D finite biaxial photonic crystal,” *JOSA A*, Vol. 24, 2710–2718, 2007.
38. Tayebi, B., J. H. Han, F. Sharif, M. R. Jafarfard, and D. Y. Kim, “Compact single-shot four-wavelength quantitative phase microscopy with polarization- and frequency-division demultiplexing,” *Optics Express*, Vol. 25, 20172–20182, 2017.
39. García, R. C., J. O. Pinto, W. I. Suemitsu, and J. O. Soares, “Improved demultiplexing algorithm for hardware simplification of sensed vector control through frequency-domain multiplexing,” *IEEE Transactions on Industrial Electronics*, Vol. 64, 6538–6548, 2017.